The inherent fragility of collective proliferative control

Michael G. Caldwell[1] and Arthur D. Lander[1,2,3,*]

[1]Center for Complex Biological Systems, [2]Department of Developmental and Cell Biology, and [3]Department of Biomedical Engineering, University of California, Irvine, CA 92697-2300

*corresponding author; adlander@uci.edu

ABSTRACT

Tissues achieve and maintain their sizes through active feedback, whereby cells collectively regulate proliferation and differentiation so as to facilitate homeostasis and the ability to respond to disturbances. One of the best understood feedback mechanisms—*renewal control*—achieves remarkable feats of robustness in determining and maintaining desired sizes. Yet in a variety of biologically relevant situations, we show that stochastic effects should cause rare but catastrophic failures of renewal control. We define the circumstances under which this occurs and raise the possibility such events account for important non-genetic steps in the development of cancer. We further suggest that the spontaneous stochastic reversal of these events could explain cases of cancer normalization or dormancy following treatment. Indeed, we show that the kinetics of post-treatment recurrence for many cancers are often better fit by a model of stochastic re-emergence due to loss of collective proliferative control, than by deterministic models of cancer relapse.

INTRODUCTION

Animal species depend for survival on the ability to build and maintain tissues that are stable (relatively unchanging in time) and robust (near in size and morphology to a desired set-point). Among other things, achieving these goals requires a mechanism for proliferative homeostasis, a process typically carried out in the context of cell lineages—i.e., the production of differentiated or "terminal" cells by stem cells or stem cell-derived intermediate progenitors. Although it is widely understood that homeostasis must, at some level, amount to a process of matching the production of terminal cells to their turnover, surprisingly little is known about how this is accomplished across the multitude of tissue types.

In recent years, mathematical models have helped elucidate fundamental mechanisms underlying stem cell behavior and tissue growth[1-7]. Here we exploit such models to identify tradeoffs that tissues may encounter in attempting to achieve homeostasis. In particular, we investigate the possibility that control mechanisms that evolved to ensure tight homeostasis are also a source of fragility, so that, on vary rare occasions, one may expect well-controlled tissues to spontaneously start growing without bound.

To the extent such a fragility exists—we will argue that it is likely unavoidable—understanding how tissues minimize it can shed light on the constraints under which normal tissues operate. Perhaps even more importantly, understanding how such a fragility arises can suggest new ways to think about cancer—a situation defined by the absence of controlled growth. Cancer initiation is often portrayed of as the result of genetic changes that "drive" growth or "inhibit" cell death, but if homeostasis is controlled through feedback (and we argue here that it must be), one would not generally expect quantitative adjustments to such drives to produce a total collapse of control. In contrast, if total collapse can occur on its own at random, then an alternative way to think about oncogenes and tumor suppressor genes is as factors that make such rare transitions more likely.

Here we use simulation and mathematical analysis to show that a relative common form of homeostatic feedback control necessarily creates opportunities for rare, stochastic escape, particularly when the spatial constraints of cells and tissues are taken into consideration. At the heart of this behavior lies a stochastic transition that is collective, rather than cell-autonomous.

Although we do not currently know whether the development of some cancers depends upon the existence of this transition, we argue that its inherent reversibility could explain how some treated cancers become dormant, re-emerging stochastically at a much later time. Using clinical data on the timing of cancer recurrence in patients treated for a variety of different cancers, we show that recurrence kinetics are, indeed, often better fit by a model based on stochastic re-emergence than by traditional, deterministically motivated models.

RESULTS

Producing or maintaining reliable tissue size requires feedback control

Maintaining self-renewing tissues, such as blood, skin and intestinal epithelia, at fixed sizes requires stem cells to replace differentiated, or "terminal", cells at a rate matching cell turnover. It is widely recognized that to replace terminal cells at a constant rate exactly half the offspring of stem cell divisions must remain stem cells—any more and a tissue will grow in size indefinitely; any fewer and it would shrink and disappear.

Less appreciated is that fact that, even if every stem cell did renew with probability exactly equal to one half, homeostasis still could not be effectively maintained. The reason is that, for most types of stem cells, division outcomes are probabilistic, meaning that sometimes cell division produces two stem cells (symmetric renewal), sometimes two differentiated cells (symmetric extinction), and sometimes one of each (asymmetric division). Even if renewal exactly balances symmetric extinction, fluctuations induced by the probabilistic nature of these outcomes will induce, in any finite-sized population, a variance in population size that grows indefinitely over time. This is illustrated in Figure 1A, which simulates scenarios that all start with the same number of stem and terminal cells, and in which each stem cell offspring differentiates independently and

probabilistically, with probability of exactly one half. Although the average cell number across simulations remains roughly constant, the variance grows without bound (also see Appendix).

Of course, this behavior can be avoided if all stem cell divisions are asymmetric, but the fact that few stem cell systems undergo strictly asymmetric division implies that variance must get stabilized by some other means. That in turn implies that stem cells cannot behave independently of each other, a conclusion also supported by direct observation of fluctuations in systems sustained by small numbers of stem cells (e.g. [8, 9]). Specifically, stem cells must adjust their renewal behavior in response to changes in tissue size, or some proxy for tissue size, such as terminal cell number, degree of cell crowding, net rate of growth, availability of a limiting nutrient, etc. In other words, *stem cells must be feedback-controlled*.

One of the simplest and most efficient ways to achieve such control is for stem cell renewal probability to fall (i.e., for differentiation probability to rise) with the number of terminal cells, a feedback strategy that has been termed "renewal control" [5]. Renewal control has been documented in several tissues including muscle, sensory epithelia, and blood, wherein the concentrations of secreted factors (often members of the TGFβ superfamily) serve as a proxy for differentiated cell number[2, 4, 10-12]. Renewal control not only suppresses fluctuations (Fig. 1B), it displays a property known as "perfect robustness" or "robust perfect adaptation" [13], whereby the steady state number of terminal cells becomes independent of all parameters that lie outside of the feedback loop itself—for example the rate of the cell cycle, the rate at which terminal cells die, or the initial number of cells that the system begins with [4, 14-16]. Robust perfect adaptation arises because renewal control is an example of integral negative feedback, a strategy widely

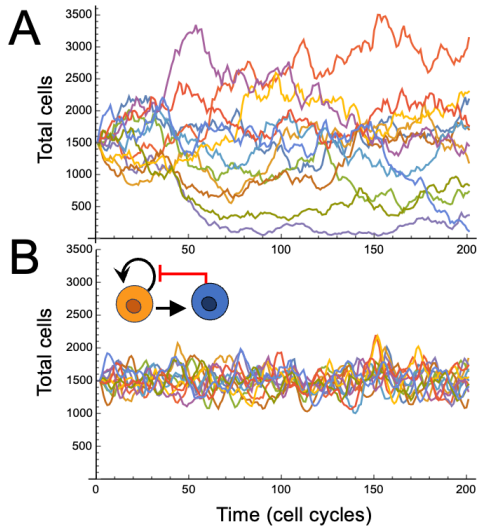

Figure 1. Monte Carlo simulations of stem cell systems **A.** Starting from an initial state of 500 stem and 1000 terminal cells, stem cells divide every cell cycle, each differentiating with probability ½, and terminal cells die at a rate of 0.5 per cell cycle. Each trace is an independent simulation. **B.** Stem cells renew probabilistically, but the probability of renewal is a declining function of the number of terminal cells, with feedback strength adjusted to produce an average terminal cell number of 1000. Initial conditions and terminal cell turnover are as in panel A.

used in both biology and engineering to maintain systems at fixed set-points in the face of unpredictable disturbances [17].

Renewal control provides a simple explanation for the extraordinary capacity of self-renewing tissues to grow and regenerate to genetically-specified sizes without any fine-tuning of initial conditions or parameters. Renewal control can also explain the robust development of non-self-renewing tissues—e.g. brain, retina, cartilage, etc.—which can be modeled as instances of renewal control in which terminal cells do not turn over: As terminal cells accumulate, net stem cell renewal eventually falls below 50%, leading to stem cell exhaustion, and a static "final state" (as opposed to a steady state) where only non-dividing cells remain. As long as such a final state is much larger than the initial state, it can be shown that the final state is nearly perfectly robust to initial conditions, as well as to other parameters lying outside the feedback loop[5, 14].

Figure 2 illustrates the flexibility and robustness of renewal control in both steady- and final state contexts. Panels A and E diagram feedback circuits in which terminal cells (blue) that either do (A-D) or don't (E-H) turn over inhibit the renewal of stem cells (orange). B and F show the solutions to (deterministic) differential equations, for a single set of parameters, in which cells are represented as continuous concentrations, and feedback follows a declining Hill function (i.e., a function that, with enough terminal cells, would drive stem cell renewal to zero); notice how steady and final states are reached, respectively, in these two cases. In panels C and G, solutions to the same equations are presented using a phase diagram, with stem and total cell numbers on the two axes, and time represented by arrows on streamlines. From these panels one can see how solutions that start from different initial conditions evolve to converge on a single fixed point (panel C) or small region on the ordinate axis (panel G). Panels D and H show the outcomes of stochastic simulations similar to those in Fig. 1—cases in which cells were treated as discrete units undergoing probabilistic divisions—and the results of 500 such simulations are plotted using phase diagrams (as in C and G). Although the stochastic and deterministic trajectories are attracted to similar locations on the phase diagram, it is clear that stochasticity allows for oscillations about the deterministic steady state, a phenomenon also apparent in Fig. 1B.

Stability and instability in the feedback control of growth

Any biologically useful strategy for controlling tissue size must produce a stable steady state (or, when needed, a final state). The ideal strategy should be globally stable, i.e., stable regardless of parameter choices, since that would ensure that disturbances to parameters (e.g., mutations that affect gene expression) could not easily lead to uncontrolled growth. The equations that govern the behaviors depicted in Fig. 2A-H are, in fact, globally stable. However, as with most simple models, the equations rely on simplifying assumptions. For example, representing feedback with a declining Hill function is arbitrary. As it turns out, global stability would still be guaranteed if feedback were represented by any monotonically declining function that preserves the potential to drive the renewal probability from above ½ to below ½. A more serious issue is the assumption that the behaviors of stem cells (or the probabilities associated with those behaviors) depend only on

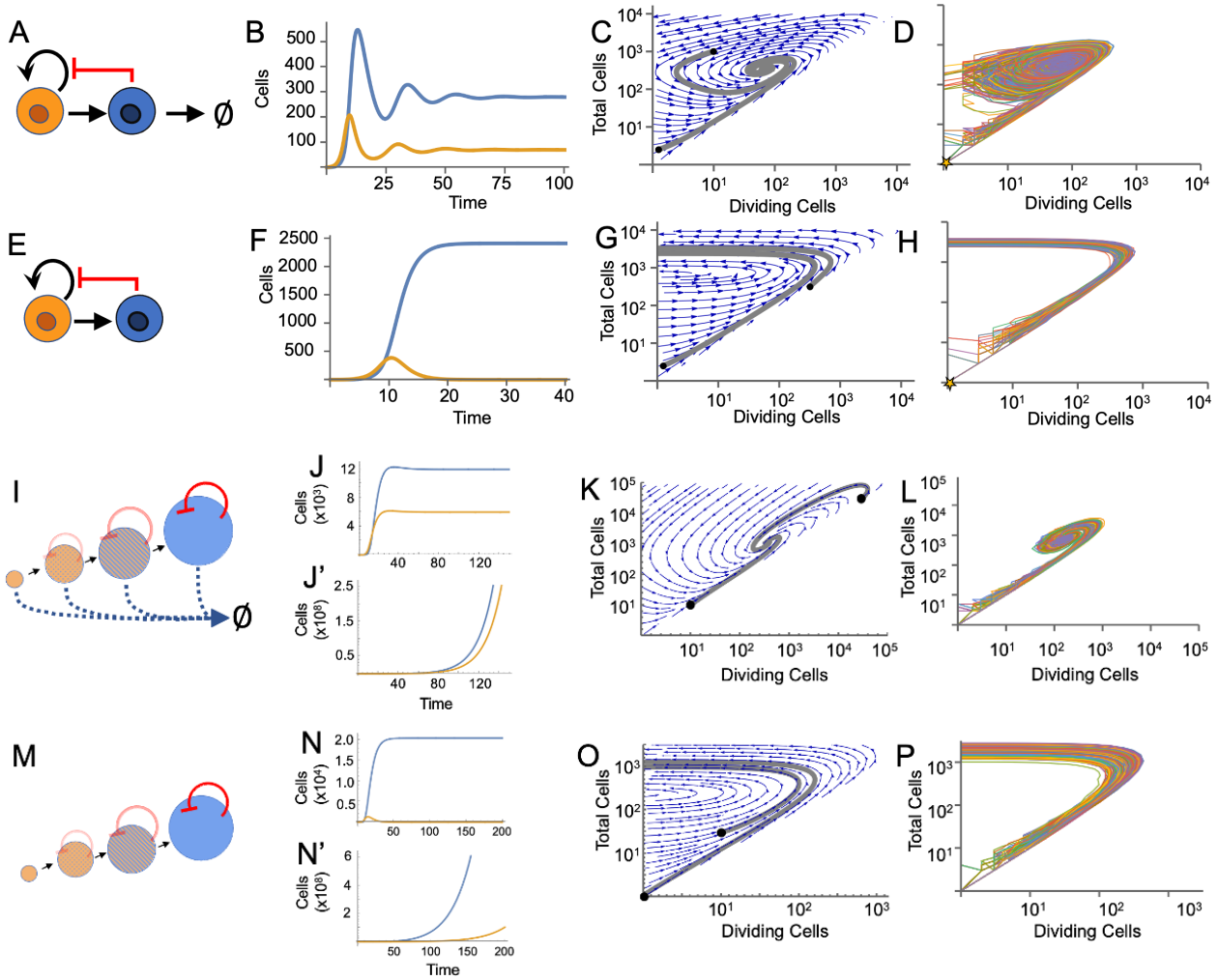

Figure 2. Behaviors enabled by renewal control. A-D. Feedback inhibition of stem cell renewal by long-lived terminal cells produces a robust steady state. Ordinary differential equations that model the feedback circuit in A were solved for a single set of parameters in B-C. In A-B, orange denotes stem cells and blue terminal cells. Panel C plots solutions in the phase plane. In D, 500 Monte Carlo simulations were performed in which differentiation of stem cell offspring was probabilistic. **E-H.** Feedback inhibition of stem cell renewal by terminal cells that do not turn over produces a robust final state. Panels were generated as in A-D. **I-P.** Simplified models of renewal feedback in solid tissues, taking into account declining sensitivity to feedback as tissues grow beyond the characteristic decay length of a diffusing feedback signal. I-L represent the steady-state case; M-P the final-state case (no terminal cell turnover). Alternative panels J-J' and N-N' display stable (J, N) and unstable (J'-N') behaviors for different parameter sets. Phase plane results are shown in K and O and stochastic simulations in L and P. For parameter values, see Table 1.

time, and not space, i.e., stem cells all receive the same feedback regardless of location. In reality—in solid tissues at least—stem cells at different locations would likely be exposed to different levels of feedback signals. For example, if such signals are carried by diffusible molecules, concentration gradients should arise.

The stability behavior of such systems is better modeled using partial differential equations, but their analytical treatment is complicated[18]. To build intuition more easily, we considered an intermediate formulation that still uses ordinary differential equations (ODE) and accounts for spatial effects in a simplified manner. Specifically, we modeled a solid tissue as a growing disc in two-dimensions, the area of which is determined by the number of total (stem and terminal) cells. We assume stem and terminal cells are uniformly mixed ("well stirred") within the disc (we relax this assumption later). At every location, we consider that a negative feedback signal is produced in proportion to the local concentration of terminal cells, and that the carrier of this signal diffuses away, and is taken up (or destroyed) at a constant rate. Assuming diffusion and uptake are fast relative to tissue growth, we may convert the spatial pattern of production of the feedback signal into a steady-state concentration gradient across the disc. As described elsewhere[19], that shape may be calculated exactly, and has the expected property of being highest in the center of the disc and lowest at the edge. Accordingly, the amount of feedback "felt" by stem cells will differ by location. To obtain an expression for the aggregate behavior of the entire stem cell pool, one integrates the renewal probability across the disc, deriving an. average renewal probability. The time-evolution of the total numbers of stem and terminal cells from any initial condition may then be formulated as an ODE problem.

Figure 2I-P explores the behavior of such systems for cases in which terminal cells do (Fig. 2I-L) and don't (Fig. 2M-P) turn over. In both cases they are no longer globally stable. When feedback is sufficiently strong, steady or final states are reached (Fig. 2J and 2N), but with weaker feedback, unbounded growth occurs (Fig. 2J' and 2N'). This is because, as such systems expand they experience "declining gain feedback", where the total feedback produced by the system does not rise fast enough to keep pace with system growth. This happens because gradients created by diffusing substances produced within a spatial domain always approach a saturating shape as domain size becomes large relative to the intrinsic decay length set by the parameters of diffusivity and decay [19].

On the other hand, such systems are still locally stable, so that if one chooses parameters appropriately, they behave similarly to non-spatial models, exhibiting robust perfect adaptation of steady states and near-perfect adaptation of final states (Fig. 2K, O, respectively). Importantly, stochastic trajectories in these regimes closely mirror deterministic ones.

Stochastic instability can arise when cell types do not thoroughly mix

Of course, solid tissues do not grow as perfect discs or spheres, nor do cells normally intermingle perfectly. To investigate the consequences of a more realistic accounting of spatial details, we turned to agent-based modeling. In such models each cell and its behavior are represented explicitly, so stochastic effects are automatically captured. Fig. 3A-B shows the rules of an agent-based model in which cells divide on a grid, pushing their neighbors aside as they do; terminal cells arise but do not turn over; and the probability that stem cell offspring renew (as opposed to differentiate) decreases according to a diffusion gradient created by the release of a feedback signal from each differentiated cell (see methods).

Simulations were initialized with a square of 4 cells, two dividing atop two differentiated cells, and run until either all divisions stopped, or the number of stem cells exceeded 70,000. Fig. 3C summarizes the results of 5,000 simulations, and shows that the vast majority ran out of dividing cells, stopping with a median size of 39 cells. They formed a roughly log-normal distribution of final sizes, with 99% of cases stopping at fewer than 420 cells. These simulations qualitatively mirrored the behavior in Fig. 2P, although the final size in this case was considerably smaller.

Three cases, however, continued to grow on what appeared to be an exponential trajectory. Fig. 3D contrasts the behaviors of 6 typical cases with one of the three that failed to stop growing, displaying the arrangements of cells after 4 cell cycles and, below that, at the end of the simulation.

Such spontaneous escape from growth control was never seen in simulations of any of the models in Figure 2. Given the patchy appearance of the continually-growing simulation in Fig. 3D, we reasoned the difference had to do with cell mixing. In the agent-based model, cells only move when they are pushed by newly generated cells, whereas in Fig. 2I-P it was assumed that cells were well-stirred. To test whether an absence of cell mixing could explain rare stochastic escape, we modified the ODE models in Fig. 2, mandating that stem and terminal cells always and instantaneously sort away from each other (this allows the model to still be posed in terms of ODEs). Fig. 4A-F shows the results when stem cells were made to sort to the outside of growing discs; in Fig. 4G-L, stem cells all moved to the interior.

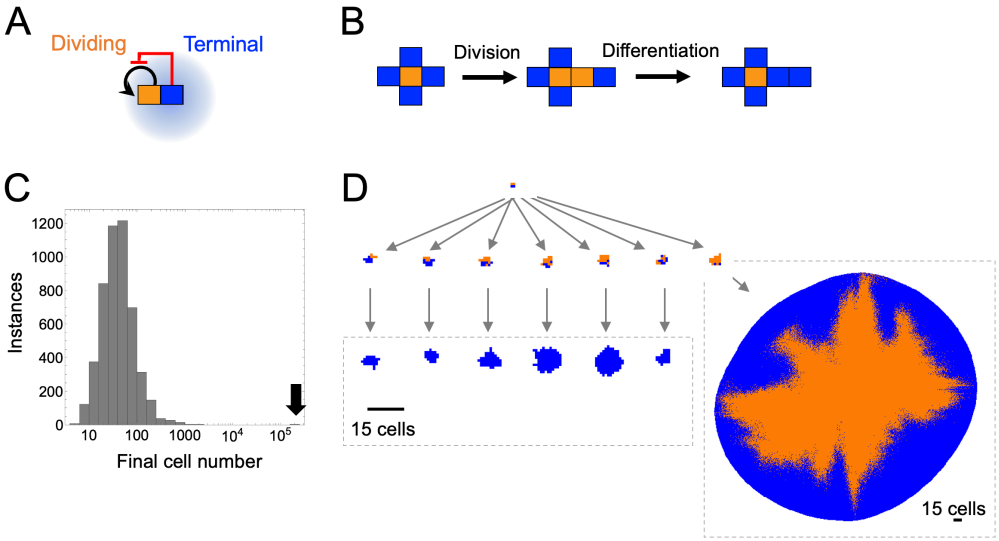

Figure 3. Rare occurrence of spontaneous stochastic instability. An agent-based model was used to simulate cells growing and differentiating in a two-dimensional space, under the influence of renewal feedback. **A-B.** Cells were initialized on a fixed grid, and diffusion gradients from each differentiated cell were calculated and summed to produce a feedback field, from the which probabilities of differentiation at each position were calculated. Starting from initial conditions of two dividing cells juxtaposed with two differentiated cells, simulations were run until either no dividing cells remained, or the number of dividing cells exceeded a pre-set maximum. **C.** Distribution of final sizes produced by 5000 simulations. The arrow indicates rare simulations that were stopped because dividing cell numbers exceeded 70,000. **D.** Images from 6 representative simulations that had ceased growing, and one of the three that had not. The initial condition for all simulations is shown at the top, the results after 4 rounds of cell division in the middle, and the results at the end of simulation at the bottom. The image at the right (note smaller scale bar) reached 92,998 dividing and 70,768 differentiated cells after 25 cell divisions.

When the equations describing these scenarios were analyzed using phase diagrams (Fig. 4B,E,H,K), biomodality was noticed: For a single set of parameters, the same system could be attracted either to a stable state or undergo unbounded growth, depending on the initial conditions (depicted as black dots on the phase diagrams). In general, conditions that grew without bound were those that started with an already large number of stem cells.

Whereas initial conditions fully determined the outcomes of deterministic solutions, stochastic simulations starting from conditions that were expected to lead to stability occasionally ended in unbounded growth (such trajectories are shown in black in Fig. 4C,F,I and L). This is just the sort of behavior that was seen in Fig. 3. By plotting stochastic trajectories onto the models' phase diagrams, it could be seen that escape from control arises when fluctuations allow the system to cross, on occasion, the separatrix that divides the two possible modes of behavior.

The cartoon in Fig. 4M provides a rationale for such behavior. Here stem (orange) and terminal (blue) cells are envisioned growing in one dimension, with terminal cells sorting automatically to the outside of the domain. The gradient of a diffusible feedback factor produced by terminal cells is depicted as blue dots. If, during any cell cycle, the size of the stem cell domain increases, then the average level of feedback within it will fall. The fall will be particularly large when the size of the stem cell domain exceeds the characteristic decay length of the diffusible factor. Since less feedback means more renewal, the chance that the stem cell domain will grow even larger in the next cell cycle goes up. That will lower feedback even further, further elevating renewal, until unbounded growth ultimately ensues. In effect, spatial inhomogeneity generates a cryptic positive feedback loop.

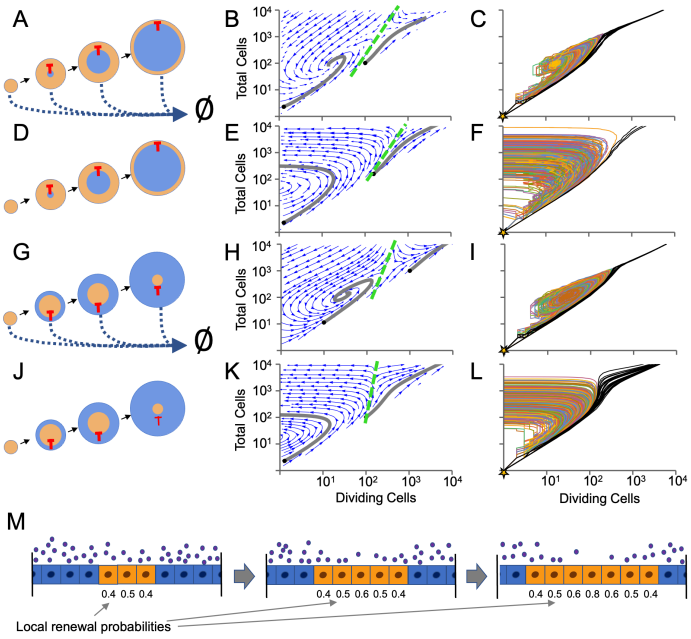

Figure 4. Cell sorting predisposes stochastic instability. **A,D,G,J**. Each row represents a system in which dividing cells (orange) grow as discs in space, and generate differentiated cells (blue), under the influence of diffusible negative feedback, modeled as in Fig. 2 panels I and M. In A and D, dividing cells instantaneously sort to the insides of discs; in G and J they sort to the outsides. In A and G, differentiated ells turn over; in D and J they do not. **B,E,H,K**. Phase portraits calculated for each of the four systems; not the appearance of a bifurcation in each case (separatrices are shown as green lines). **C,F,I,L.** 500 stochastic trajectories of each system, starting from identical initial conditions (a single dividing cell), plotted in phase space. Trajectories that spontaneously escape from growth control are shown in black. **M.** Diagram explaining the source of cryptic positive feedback. If regions containing stem cells randomly grow large enough, cells in their centers will experience reduced negative feedback, favoring further growth of such regions. See Table 1 for parameter values.

In Fig. 4, spatial inhomogeneity was enforced by the model itself (which assumes perfect cell sorting), but it is almost certainly the same phenomenon that accounts for stochastic escape in agent-based modeling (Fig. 3), where cell sorting was not mandated. This is because fluctuations in the outcomes and directionality of stem cell divisions should lead, at random, to the creation of small islands disproportionately populated with stem cells and others disproportionately populated with terminal cells. Should any one of the stem cell islands get large enough (compared with the characteristic decay length of the feedback signal), and should the average self-renewal probability within such a domain exceed ½, then effectively the same cryptic positive feedback loop as in Fig. 4 could exist.

Positive feedback on self-renewal is sufficient to generate stochastic instability

Dynamical systems with more than one attractor state are often generated by circuits that incorporate positive feedback, sometimes combined with negative. Indeed, the behaviors of renewal control systems that utilize both positive and negative feedback on self-renewal have previously been analyzed [14]. Under appropriate conditions, such systems can be bi-stable—i.e. admitting of two stable steady states (or two possible final states).

Here we show that, under other conditions (different relative strengths of the two types of feedback), such systems can be bi-modal, producing either stability or unbounded growth, depending on the initial conditions: In Figure 5, cell dynamics

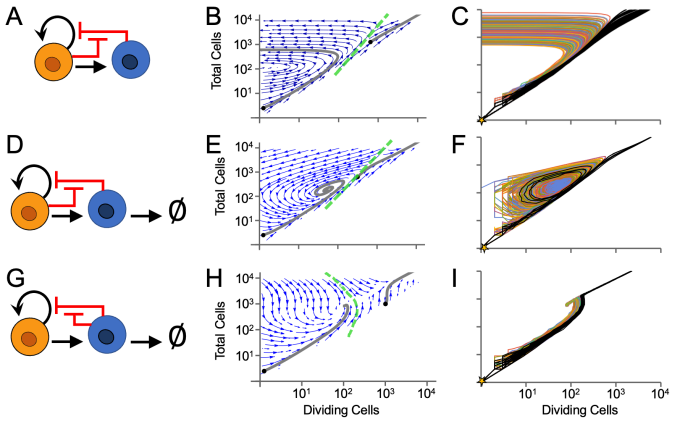

Figure 5. Positive feedback allows for stochastic escape from growth control. Each row presents the analysis of one of the mixed positive-negative feedback models in **A, D, and E.** Phase portraits are shown in **B, E, and H,** and stochastic trajectories (500 instances) are plotted in the same phase space in **C, F and I**. Trajectories that escape growth control are shown in black. Initial conditions consisted of a single dividing cell. See Table 1 for parameter values.

were modeled using ODEs (space was not explicitly considered), and positive feedback on stem cell renewal was directly introduced, with the source either being stem cells themselves (Fig. 5A-F), or terminal cells (Fig. 5G-I). For simplicity, positive feedback was modeled as inhibition of negative feedback, although other formulations are possible[14].

The results indicate that, for appropriate parameter values, mixed negative-positive feedback systems can all be bimodal, exhibiting phase diagrams much like those in Fig. 4. Moreover, stochastic simulations that started from initial conditions expected to achieve stability occasionally displayed complete loss of control, much as was also observed in Figures 3 and 4. Examination of the trajectories that escaped control suggests that, as in Figure 4, they did so because stochastic fluctuations drove them across the separatrix that divides the phase diagram into regimes of controlled and uncontrolled growth.

Reversibility of collective transitions

When thinking about rare, catastrophic events of unbounded cell proliferation, cancer naturally comes to mind. Although cancers have long been recognized as resulting from stochastic events, the traditional "multi-hit model" of carcinogenesis equates such events with the mutation of oncogenes or tumor suppressor genes[20, 21]. Increasingly, it has been recognized that changes of a non-genetic nature, such as a cell randomly flipping between epigenetic states, could also account for steps in cancer progression, and possibly also cancer initiation[22, 23]. In the cancer literature, non-genetic state changes are nearly always described in cell-autonomous terms, i.e., as something that happens to a single cell, much like mutation[22]; indeed use of the term "epimutation" to describe such events has become common [24, 25].

Collective stochastic transitions—i.e., "tipping point" phenomena that arise out of fluctuations in collective behavior—are relatively common in organismal biology[26], and are sometimes studied in developmental biology[27], but have received little attention by cancer biologists (for an exception see [28]). A unique feature of such transitions is their propensity for reversibility in response to changes in collective circumstances. For example, if a tumor had escaped growth control through a collective transition, as modeled in Fig. 3-5, one might expect to be able to return those cells to homeostasis just by altering their numbers or spatial arrangements. In essence, if stochastic fluctuations drove crossing of a separatrix from controlled to unbounded growth, then an appropriate change of circumstances should be able to drive cells back

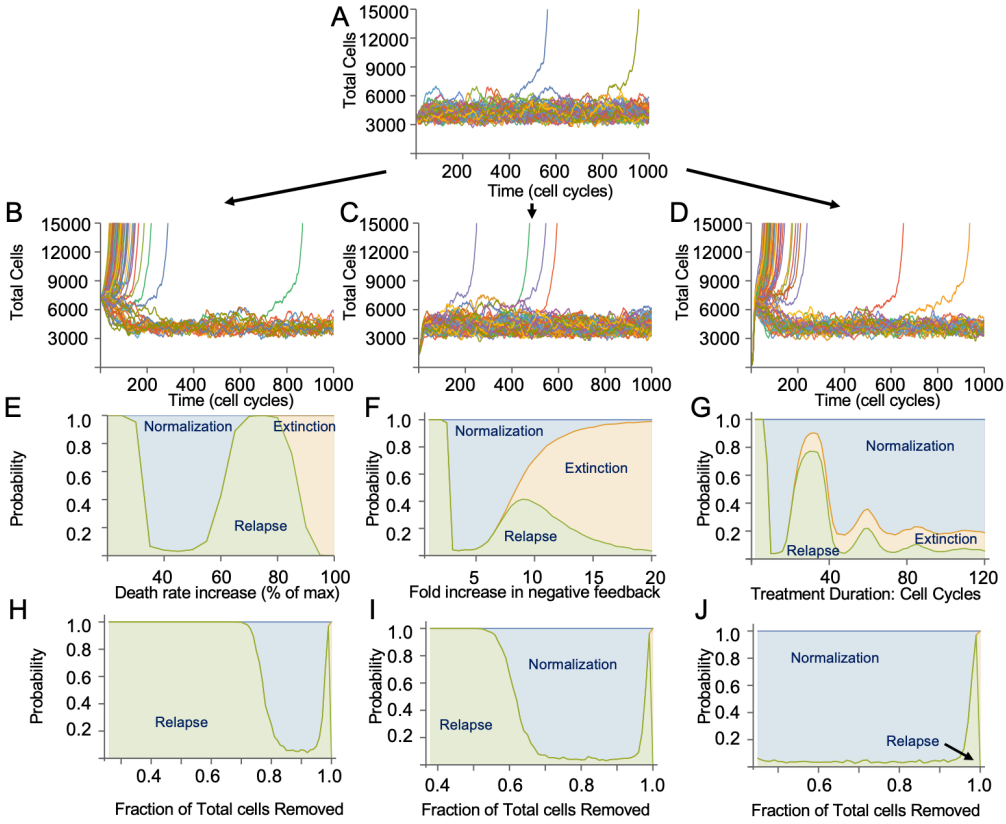

Figure 6. **Transient treatments can reverse stochastic escape from growth control. A.** 100 stochastic trajectories of the model in Fig. 5G initialized near steady state showing rare (~1-2%) escape from growth over course of 1,000 cell cycles. **(B-D)** Simulations initialized above (B), somewhat below (C), and well below (D) steady state. Note the high level of early "relapse" in B and D. (**E-G)** Simulations were initialized from a high level (15,000 cells, of which 50% were stem cells) and then subjected to various "treatments", i.e., temporary or persistent changes to parameters, to determine the fraction of trajectories that normalized (returned to steady state), relapsed, or went entirely extinct, over the course of 1,000 additional cell cycles. In (E) treatment consisted of increasing the probability of death of dividing and terminal cells, by the indicated amount, for 5 cell cycles. In (F) treatment consisted of increasing the strength of negative feedback by indicated factor for 5 cell cycles. In (G) negative feedback was increased by a factor of 1.5 for the indicated number of cell cycles. **H-J.** Simulations were initialized as in E-G, and treatment consisted of a one-time removal of the indicated fraction of total cells, but with the removed cells having different proportions of stem vs. terminal cells. In (H) the proportion was 1:2; in (I) it was 1:4 and in (J) it was 1:9.

across that same separatrix.

Simulations support this intuition. In Figure 6 the underlying model was, for convenience, the mixed positive-negative feedback model of Fig. 5G. Panel A shows 100 trajectories that all initiated from near the deterministic steady state for this system, at 4,000 total cells (700 dividing and 3300 terminal). Notice how two trajectories randomly "escape" control and start to grow without bound (similar to the black trajectories in Fig. 5G). To mimic cancer treatment we started from the point at which one of the escaped trajectories had reached 15,000 cells, and then removed a fixed number of those cells (both dividing and terminal), in the process driving the system to the other side of the separatrix shown in Fig. 5H.

Simulation was then re-initiated from initial conditions in which cell removal had driven the system to a point where total number was either above (panel B), somewhat below (panel C) or far below (panel D) the predicted (deterministic) steady state (see figure legend). In all cases, a large proportion of the ensuing trajectories returned to tightly controlled fluctuations, indicating resumption of homeostasis. At long times, all three conditions behaved similarly, with occasional trajectories re-escaping from control, however their short-term behaviors differed. In B, a large proportion of trajectories returned quickly to unbounded growth, whereas that did not occur in C, Interestingly, panel D exhibited an early burst of escaping trajectories like those in panel B. The early escapes in B undoubtedly reflect of the fact that the initial condition was sufficiently close to the separatrix that random re-crossing was relatively likely. The early escapes in D, however, reflect a different phenomenon: the inherently oscillatory nature of renewal control[5], which causes perturbations that go too far below a steady state to elicit compensatory overshooting. Such overshoots enable a large proportion of trajectories to make close approaches to the separatrix, again allowing for a high probability of stochastic re-crossing.

The abrupt removal of a large fraction of the cells from an escaping simulation might be seen as a model of tumor treatment by surgical removal or ablation. As many cancers are treated non-surgically, e.g., with various dosing schedules of radiation, chemotherapy, or immunotherapy, we asked whether those kinds of treatments might also be expected to "normalize" the behaviors of growth-escaped cells. The results are summarized in Fig. 6E-J, in which the strength or duration of treatment is varied on the abscissa, and the ordinate shows the fraction of trajectories that either resumed homeostasis ("normalization"), fluctuated to zero ("extinction") or exhibited early resumption of uncontrolled growth ("relapse").

As can be seen in Fig. 6E-G, maximal normalization often occurs at relatively low treatment strengths, giving way to a high level of relapse at treatment strengths that begin to produce a large amount of extinction. Interestingly, whereas minimizing relapse with short term treatments requires fine-tuning treatment strength, it appears that low-intensity treatment over a long duration often does equally well. Although these results come from the exploration of a rather simplified, "toy" model, it is intriguing that they predict a phenomenon that has been observed in the clinic, which is that long-duration treatment of cancers with low dose chemotherapeutic agents (so called "metronomic therapy") sometimes achieves surprisingly good results[29-32]. Results in Fig. 6H-J further show that the success of ablative therapies can depend strongly on which type of cell is primarily being ablated—dividing cells or their non-dividing (or slowly dividing) offspring.

Are signatures of stochastic instability present in clinical data?

The analyses above suggest that, for cancers in which the final step in malignant transformation is a collective, stochastic transition, tumor treatment might sometimes work because malignant cells return, at least temporarily, to homeostatic growth. In fact, there are some striking examples of cancer normalization in animal models[33-35], as well as rare human tumor types that spontaneously normalize without treatment[36]. There is also growing recognition that very late recurrences of tumors following treatments intended to be curative reflect "dormant" residual disease. Although mechanisms underlying dormancy are unknown[37], it likely involves at least some degree of restoration of normal cell behavior.

It is improbable that normalization would occur by chance reversion of mutations (or epimutations) that act in a cell-autonomous fashion. Even if back-mutation (or back-epimutation) were not exceedingly rare at the level of the individual cell, the need for multiple cells to undergo such an event at the same time would typically preclude success. But with collective transitions that should not be the case. As Fig. 6 shows, systems that have escaped growth control collectively ought to be returnable to steady state solely by transiently removing enough cells or transiently adjusting the parameters of feedback.

Does this ever happen when cancers are treated? One way to investigate this is to examine the kinetics with which tumors recur after treatments that were intended to be curative. If, following treatment, residual tumor cells undergo normalization through reversal of a collective transition, then the kinetics of recurrence should match those of a random process. This is illustrated by Fig. 7A-C, in which we simulated what happens to stochastic trajectories produced by the model in Fig. 6 after "treatment" (removal of a large number of cells). With sufficiently long follow-up, trajectories restored to homeostasis re-escape at times that exactly follow an exponential distribution (Fig. 7B-C). Exponential waiting times are the hallmark of a "single-hit" stochastic process, as they are the reflection of a probability rate (as known as a hazard rate) that is constant in time.

A considerable amount of clinical data exist on cancer recurrence kinetics, and there is also a large literature on modeling recurrence. Here we are specifically concerned only with situations in which cancers were treated with curative intent, and followed with as little additional treatment as possible (i.e., we exclude scenarios in which recurrence would be driven by therapy-resistant cells emerging by new mutation during prolonged treatment). Unless a random event drives recurrence, patient-to-patient variation in recurrence time would need to be explained by differences in initial conditions or parameters. For example, patients are likely to vary in the size of tumor residua after treatment, as well as the rate at which tumors grow. Because the distributions of those parameters are necessarily bounded, it is not generally possible for variation in them to produce a recurrence probability rate that is constant in time.

We wondered whether an analysis of recurrence data for a variety of different cancers might identify ones in which a simple,

single-hit stochastic model is a substantially better fit than deterministic ones. In Figures 7D-N and Supplemental Fig. 1, we tested this on 24 data sets representing 14 different cancers (Table 2). For the single-hit, stochastic model, three parameters were fit to the data: a transition probability rate, a time lag between when the stochastic event occurs and when tumors are detected, and a fraction of patients not at risk (i.e. patients that had been cured). Of the latter two parameters, the time lag was often negligible and an estimate of the fraction cured was often obvious from the data, however values were obtained by fitting nonetheless. For deterministic models, we fit two parameters—representing the mean and variance of either the sizes of tumor residua or the exponential rate constants of tumor re-growth—as well as the fraction of patients not at risk (see Methods for further details).

As Fig. 7 shows, for several solid cancers—notably renal, hepatocellular, prostate, ovarian, and basal cell carcinoma—the single-step stochastic model was a substantially better fit to the data than either of the deterministic models, whether judged by manually inspecting residuals (see insets) or using Akaike or Bayesian information criteria (Fig. 7J and S1). In contrast, some data sets were reasonably fit by all models, including melanoma, several types of breast cancer and acute lymphocytic leukemia.

Some data sets were poorly fit by all models. In the case of chronic myeloid leukemia, recurrence data were distinctly biphasic (see arrow in L), suggesting that subsets of patients recur by different mechanisms. For ER+ and ER- breast cancers, no model provided a good fit, perhaps because these designations include more than one type of cancer.

As summarized in Fig. 7N, whenever we could find additional clinical studies on the same cancers as those in Fig. 7D-M, the results came out similarly (Fig. S1). For example, in all three renal carcinoma and both hepatocellular carcinoma data sets, the single-hit stochastic model was a consistently a better fit than the other two. In a second ovarian data set (based on an older patient cohort) the stochastic model was nearly as good as the best deterministic one. With other breast and leukemia datasets, in contrast, results were similar to those in Fig. 7, even in cases in which no model provided a good fit. From these observations we conclude that the different shapes of recurrence curves for different cancers are specific to the cancer

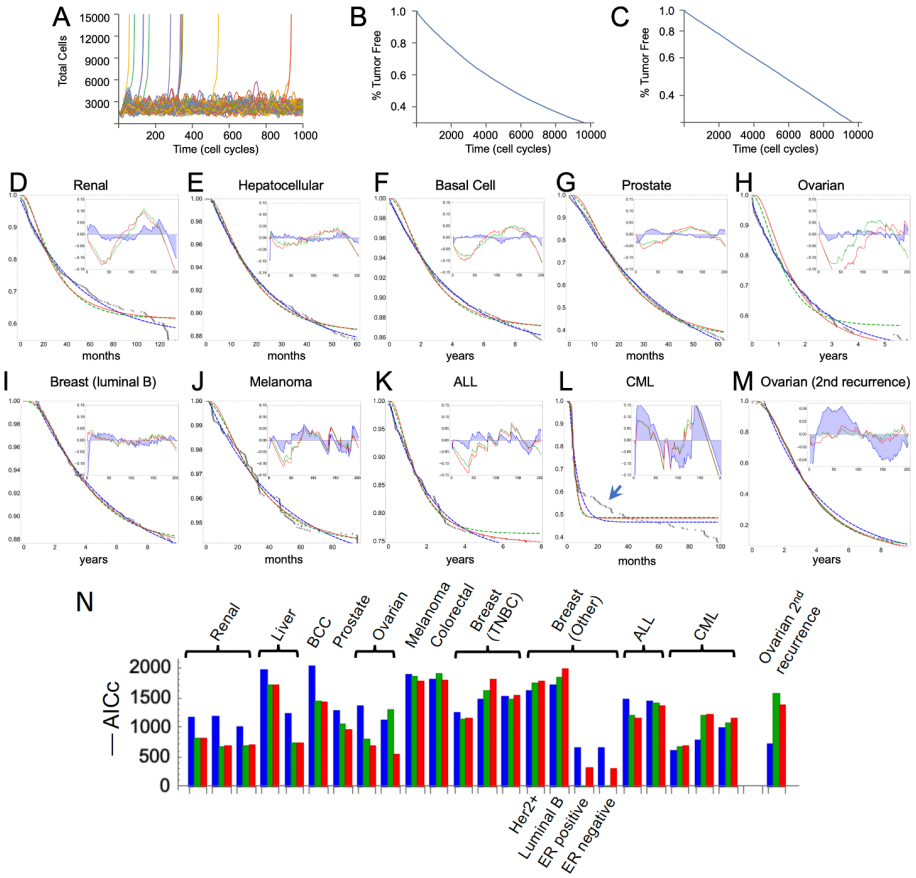

Figure 7. Single-hit kinetics in cancer recurrence. A. 100 stochastic trajectories of the model in Fig. 5G initialized near steady state run long enough to observe ~12% escape. **B-C.** Escape-free survival (defined as never exceeding 100,000 total cells) as a function of time, for 25,000 simulations from the same initial conditions as those in A. Axes are linear in B and logarithmic in C. **D-M.** Kaplan-Meier curves are shown for cancer recurrence following surgery and/or cessation of treatment. Shown are 10 published studies (and additional 14 studies are presented in Fig. S1, and summarized in Table 1). Each curve was fit to one of three models: stochastic escape (blue line); deterministic re-growth from a distribution of initial conditions (green) and deterministic re-growth using a plausible distribution of growth-rate constants (red line). The inset in each panel shows the fit residuals for each model. To facilitate comparison between models, fit residuals were normalized to the initial at-risk fraction as predicted by the models (an average of the three). Residuals closer to zero indicate a better fit. N. Corrected Aikake Information Criterion (a global measure of goodness of fit) for all 24 data sets. Values for each model are color coded as in D-M. For details of models and fit parameters, see Methods.

types, and not just reflective of noisy data.

As a control, we also analyzed an additional large study of recurrence in ovarian cancer patients who had already recurred once before. These patients nearly all relapsed relatively quickly, suggesting recurrence was likely due to tumors regrowing deterministically from large or aggressive residua. One would not expect the kinetics of such recurrence to be well fit by a constant probability stochastic model, and that is indeed what was found. As shown in Fig. 7M, for these data both deterministic fits were much better than the stochastic one—the only data set displaying such behavior.

Discussion

The results presented here come from the analysis of theoretical models and their ability to fit clinical observations. The initial goal of exploring such models was to build intuitions about how stochastic fluctuations and feedback control of cell proliferation interact in unexpected ways. What was shown was that feedback circuitry that normally guarantees stability and robustness over a large portion of parameter space can, in the presence of positive feedback, also be the source of rare, stochastic instability.

The kind of positive feedback required to do this can be either explicit or cryptic. Cryptic positive feedback, it was shown, arises by default in any spatial system in which the spread of a feedback signal can in some circumstances not keep up with domain growth—at the very least this means any system in which feedback depends on diffusion, or any process that decays similarly over space (e.g., mechanical tension[38]). It arises particularly easily when stem cells and their differentiated offspring explicitly sort away from each other (Fig. 4) which, as it happens, is a common situation in many, if not most, epithelia, wherein stem and progenitor cells reside in a separate compartment, usually next to the basement membrane. However, as we show by agent-based modeling (Fig. 3), such a situation even arises when stem and differentiated cells simply remain near where they are born and are only moved about passively (Fig. 3).

In addition to such examples of cryptic positive feedback due to spatial limitations, there appear to be many tissues in which positive feedback can be explicit as well, through the combined actions of feedback factors that have opposing effects on self-renewal[14]. For example, tissues that use TGFβ-family molecules to feedback negatively on stem cell renewal commonly co-express MAP kinase-stimulating ligands that feedback in the opposite direction. Thus, beyond the cryptic feedback that arises due to spatial effects, there are strong reasons to expect the potential for stochastic instability to exist in renewal-controlled tissues.

Stochastic instability may thus be viewed as a generic, structural shortcoming of renewal control circuitry, at least in solid tissues. The idea that stabilizing, homeostatic feedback can be a source of instability may seem surprising, as control processes typically dampen, rather than enhance, stochastic effects (as, for example, in Fig. 1B). Such behavior nicely illustrates what Doyle and colleagues termed the "robust-yet-fragile" nature of complex control systems—where the price of good control is typically a predisposition to rare, catastrophic failures[39].

Even if self-regulating tissues cannot completely eliminate the probability of spontaneous escape from control, they are no doubt under strong evolutionary pressure to minimize it, which they could presumably do through appropriate choices of parameters (e.g., stronger negative feedback, longer decay lengths of feedback gradients). Recognizing this allows one to re-imagine cancer causing agents, such as oncogenes, as factors that merely nudge those parameters into riskier territory. This allows one to view oncogenes less as agents that deterministically cause cells to proliferate—something they clearly do not most often do, as phenotypically normal cells are increasingly being found to harbor oncogene mutations[40, 41]—and more as agents that lower the guardrails on a process already inclined, albeit rarely, to fail (in some regards this viewpoint echoes concerns raised by earlier cancer researchers that one should treat unbounded growth, not quiescence, as the "natural" state of cells[42]).

Whether collective, stochastic transitions to unbounded growth are indeed part of the process of cancer initiation and development remains to be determined empirically, but several of the modeling results presented here support that view. As shown in Fig. 6, the unique tendency of collective transitions to reverse themselves following removal of cells or appropriate changes to parameters provides both a model for cancer dormancy and an justification for the ability of metronomic chemotherapy to perform comparably to high-dose, short term treatments[29-32].

By no means do these results imply cancers should always be expected to undergo reversion after treatment. Even if collective transitions, such as those described here, play a role in carcinogenesis, subsequent cell autonomous transitions (e.g., mutations and epimutations) that are effectively irreversible would likely preclude true normalization. Still, the idea of reversion provides a conceptual framework for understanding cancer dormancy that does not require postulating the existence of a novel, cancer-specific mechanism.

As mentioned above, the hallmark of normalization by reversion of a collective, stochastic transition is that recurrence should display the kinetics of a single-hit stochastic process (Fig. 7A-C). We identified many types of cancer where published recurrence curves are consistently well-fit by such a process (Fig. 7D-N). Indeed, for renal, hepatocellular, basal cell, prostate and ovarian cancers, single-hit stochastic fits outperformed simple deterministic models in which tumor residua either varied in size or growth rate among patients.

It is important that these results not be overinterpreted. The deterministic models used here were kept deliberately simple to avoid introducing more parameters than were present in the model they were being compared with, and the distributions underlying the deterministic models were chosen somewhat arbitrarily. Still, the general point they make is that it is difficult to approximate kinetics associated with a uniform hazard rate without introducing some kind of stochastic event. Of course, that event does not have to correspond to the crossing of a separatrix created collective feedback control of growth. Indeed, others have generated empirical models of cancer recurrence in which an arbitrary number of slow, stochastic events were used to provide a good fit to data[43]. Still, given that such transitions must be relatively rare to account for broad ranges of recurrence times, it is not easy to identify many possible cellular mechanisms for producing them. Here we

identify a very simple mechanism, one that emerges spontaneously, and unexpectedly, out of the need of tissues to control their own sizes.

METHODS

Deterministic models of growth control (non-spatial)

Modeling used a lineage control framework in which differentiated cells dose dependently feedback upon the renewal probability of dividing cells – the equations for lineage control were adapted from[4] .

$$c0'(t) = c0(t)(2p - 1) \quad (1)$$

$$c1'(t) = 2c0(t)(1 - p) - d * c1\,(t) \quad (2)$$

Where *c0* is the number of dividing cells, *c1* is the number of terminally differentiated cells, *d* is the turnover rate of differentiated cells, and *p* is the probability that daughter cells created upon division remain dividing cells. When *d*>0, the system reaches a stable steady state in which dividing and differentiated cells co-exist; if *d*=0, the system reaches a final state entirely comprised of differentiated cells.

For both ODE and non-spatial stochastic models, the probability of renewal *p* was calculated in three different ways depending on what was being modeled.

In the absence of positive feedback:

$$p = \frac{p_0}{\gamma * c1^{\mathrm{n1}} + 1}$$

With positive feedback from dividing cells:

$$p = \frac{p_0}{\frac{\gamma * c1^{\mathrm{n1}}}{\phi * c0^{\mathrm{n2}} + 1} + 1}$$

With positive feedback from differentiated cells:

$$p = \frac{p_0}{\frac{\gamma * c1^{\mathrm{n1}}}{\phi * c1^{\mathrm{n2}} + 1} + 1}$$

Where p_0 is the renewal probability in the absence of feedback, γ is a constant representing the strength of negative feedback, ϕ is a constant representing the strength of positive feedback, n1 and n2 are the gains of the negative and positive feedback respectively, *c1* is the number of differentiated cells and *c0* is the number of dividing cells. Parameter values and initial conditions for all figures can be found in Table 1.

Growing disk models

To account for the effects of space on the distribution of feedback signaling without requiring the use of partial differential equations, we constructed an idealized scenario in which a collection of cells were represented as a disk, the area of which was equal to the sum of the areas of each cell. Disks then evolved according to equations 1-2, except the calculation of p depended on disk area. Specifically, we model negative feedback as being carried by a factor that is produced in proportion to the number of terminal cells in the disk, and diffuses and linearly decays, reaching a steady state diffusion gradient rapidly, relative to cell growth.

In such a situation it has been shown[19] that the steady state shape of the diffusion gradient produced is of the form

$$c(x) = v(1 - \frac{r}{\lambda} I_0\left(\frac{x}{\lambda}\right) K_1\left(\frac{r}{\lambda}\right)) \quad (3)$$

Where *c* is the concentration of the diffusing factor, *v* is its rate of production, x is radial distance from the center of the disk, *r* is the radius of the disk, λ is a constant representing the decay length of the diffusing factor, and I_0 and K_1 are modified Bessel functions of the first and second kinds, respectively. To compute a renewal probability *p* for dividing cells we integrate the value of

$$p = \frac{p_0}{1 + c(x)/k}$$

across the disk, where p_0 is the renewal probability in the absence of feedback and *k* is a constant, to obtain a single average value that is used in equations 1-2.

In cases in which dividing and differentiated cells were assumed to be well-stirred, *v* was taken to be proportional to the proportion of total cells that were differentiated.

In some simulations, disks were divided into an inner disk and outer annulus with dividing and differentiated cells assumed to sort immediately into one or the other compartment. In such cases it was necessary to use the formula for the diffusion gradient outside of a uniformly producing disk:

$$c(x) = v(\frac{r}{\lambda} K_0\left(\frac{x}{\lambda}\right) I_1\left(\frac{r}{\lambda}\right)) \quad (4)$$

If the dividing cells occupied an annulus outside a disk of differentiated cells, Eq. 4 was used directly; if dividing cells occupied a disk inside an annulus of differentiated cells we calculated equation 3 for both the inner and outer radii and subtracted one result from the other.

Stochastic simulations of lineage control

Monte Carlo models were used to reveal the effects of fluctuations in cell number due to stochastic cell differentiation and death. At each time step all dividing cells divide and the fates of their daughter cells were probabilistically determined according to the calculated value of *p* at that time step. For example, if the probability of renewal is 0.6, then each daughter cell has a 60% chance to remain a dividing cell and 40% chance to differentiate. Additionally, each differentiated cell was assigned a constant probability *d* of disappearing each time step. The order in which events were executed was:

1) The probability of renewal was computed using the current number of dividing and differentiated cells.
2) The number of differentiated cells that turnover was chosen probabilistically.
3) Dividing cells divided and the fates of daughter cells were chosen probabilistically based on the probability of renewal.

Stochastic simulations were run until no dividing cells remained, total cell numbers reached a predetermined upper limit (generally 250,000 cells), or if a predetermined number of time steps had elapsed.

Agent Based Modeling

An agent-based model was used to explore stochastic spatial effects. Simulations were carried out on an 800 x 800 grid, and initiated with two adjacent dividing cells juxtaposed with two adjacent terminal cells in the center. At each time step, cells could divide, and rules were used to determine both the fate of each offspring (renewal vs. differentiation) and how neighboring cells would adjust their positions to the extent necessary to create an open space for a newly generated cell. At each time step all dividing cells divided simultaneously, but the movements of other cells to accommodate new offspring were calculated sequentially.

The fate of every newborn daughter cell was assigned probabilistically, determined by the strength of local negative feedback field at its position. Field strength was determined by summing the diffusion fields produced by every terminal cell, each of which was assumed to be of the form

$$\frac{1}{2\lambda} I_1(\frac{1}{2\lambda}) K_0(\frac{r}{\lambda})$$

Where r is the radial distance from the terminal cell, λ is a constant representing the decay length of the diffusing factor (in units of cell diameters) and I_1 and K_0 are modified Bessel functions of the first and second kinds, respectively. Renewal probability at each location was calculated as

$$\frac{p_0}{1 + (f/k)^2}$$

where f is the field strength, γ is a constant and p_0 the renewal probability in the absence of feedback, which was usually set to 1. After the fates of new cells were assigned, space was made available by identifying the nearest unoccupied grid point to the location of each cell that divided, and then "shoving" occupied cells toward that space. If multiple unoccupied grid points were identified, one was chosen at random. If that space was at the same horizontal or vertical level as the dividing cell, shoving consisted of simply inserting an empty cell either above or below, or to the left or the right, of the dividing cell, chosen at random. If the space differed in both its horizontal and vertical coordinates, both a row and a column (which one first being chosen at random) were shoved to make space for the new cell while also filling the unoccupied point. This process was carried out sequentially (asynchronously) to allocate every newly generated cell to its own position.

Typically, simulations were run until no dividing cells remained, or dividing cell numbers grew too numerous to simulate in reasonable time frames (about 70,000 dividing cells).

Modeling tumor treatment

The stochastic model of renewal control was used to explore how rare growth control failure responds to treatment. In this case the p-value formula was as in Fig. 5G, namely:

$$p = \frac{p_0}{\frac{\gamma * c1^{\mathrm{n1}}}{\phi * c1^{\mathrm{n2}} + 1} + 1}$$

Where p_0 is the renewal probability in the absence of feedback, γ is a constant representing the strength of negative feedback, ϕ is a constant representing the strength of positive feedback, n1 and n2 are the gains of negative and positive feedback respectively, and *c1* is the number of differentiated cells. The parameters used to simulate escape for treatment can be found in Table 1.

The steady state total cell number for the parameterized model was ~4200 cells. We chose a threshold of 15,000 total cells to distinguish between stable and escaped simulations, if a simulation had > 15,000 cells it was considered to have escaped growth control.

To model treatment we initialized simulations at the escape threshold, 15,000 total cells, prior to treatment. In the first case, treatment was implemented as an increase in the turnover rate in both dividing and differentiated cells. In these stochastic models the turnover rate is a constant probability of death per cell per timestep, so the probability of death per cell per time step is bounded between 0 and 1. The treatment was implemented by linearly increasing the probability of turnover between its basal probability and its maximum as follows:

$$probability\ of\ death\ per\ cell\ per\ timestep = d + (1 - d) * treatment_strength$$

Where d is the probability of death per cell per timestep in the absence of treatment and $1 \geq treatment_strength \geq 0$ is the strength of treatment.

In subsequent panels treatment was also implemented as an increase in the strength of negative feedback. This was implemented by multiplying the basal strength of negative feedback γ by a constant as shown below:

$$p = \frac{p_0}{\frac{(treatment_strength * \gamma) * c1^{\mathrm{n1}}}{\phi * c1^{\mathrm{n2}} + 1} + 1}$$

Where treatment strength is a positive constant and γ is the strength of negative feedback in the absence of treatment.

Finally, to explore how targeting dividing vs differentiated cells during treatment effected outcomes we implicitly modeled treatment by initializing the systems as if a treatment that differentially eliminated certain cell types had occurred. To do this we first assumed there were 15,000 total cells with equal numbers of dividing and differentiated cells. Then we implemented treatment by removing a proportion of the total cells from the system and fixed the remaining cells such that they contained a fixed ratio of dividing to differentiated cells. The outcomes of treatment in terms of (dividing cells, differentiated cells) was computed as follows:

$$(\,(1 - \mathrm{treatment_strength}) * 15{,}000 * \alpha\,, (1 - \mathrm{treatment_strength}) * 15{,}000 * (1 - \alpha)\,)$$

Where $1 \geq treatment_strength \geq 0$ is the proportion of total cells that were removed and $1 \geq \alpha \geq 0$ is the fraction of remaining cells that are dividing. Both *treatment_strength* and α were chosen such that the resulting number of both dividing and differentiated cells were between 0 and 7,500.

Fitting cancer recurrence data

Cancer recurrence data were obtained from 24 published studies (see Table 1), in most cases by extracting data points directly from published Kaplan Meier curves (or their equivalent) and resampling in proportion to the estimated number of patients at each time point. Disease-free survival (as a fraction of total study subjects) was fit, using the NonlinearModelFit function of Mathematica, to each of three models.

In the first model, survival was described by a combination of a single exponential curve, and a fraction of patients considered not at risk (i.e. cured, and therefore unavailable to recur). In addition, the fit allowed for observed recurrence to be displaced by a fixed amount from actual recurrence, to account for the lag required for tumors to reach a detectable threshold and the possibility that a very small percentage of patients may relapse quickly and deterministically due to primary treatment failure. The modeled survival function was therefore

$$\rho + (1 - \rho)\alpha e^{k(-t+\psi)}$$

Where ρ is the fraction of patients not at risk and k is a rate constant. ψ accounts for detection lag and was usually separately obtained from a double exponential fit to the data; a accounts for the possibility that 1-a fraction of patients relapse

quickly and deterministically. In most cases, and particularly in those cases where this model fit data well, ψ was close to zero and *a* was very close to one (usually >0.96), implying that fit quality was primarily controlled by just two parameters, *k* and ρ.

The second model corresponds to the case in which all tumors grow at a single constant rate, but the initial size of tumor residua is drawn from a distribution. We required that the distribution be bounded between 0 and the size at which tumors would be detected, with smaller sizes being more probable than larger ones. We also required that size = 0 was excluded from the distribution, since patients who were cured were to be modeled separately, as in the first model. To meet this requirement, we used a Beta distribution with a first shape parameter =1. Since the time it takes for exponential growth to bring a tumor from size z to size w, where b is the detection threshold, will be $\frac{1}{k}ln[\frac{w}{z}]$, taking one minus the cumulative distribution function of this expression when z is drawn from a Beta distribution with first shape parameter=1 is:

$$1-(1-e^{-kt})^{-1+\frac{1}{\mu}}$$

Where *k* is a rate parameter and *μ* describes the breadth of the beta distribution (and is constrained to take values between 0 and 1/3). Taking into account patients not at risk gives a final model for the survival function of

$$\rho+(1-\rho)(1-(1-e^{-kt})^{-1+\frac{1}{\mu}})$$

The third model corresponds to the case where tumor residua initiate from a constant size, but grow at a range of rates described by first order growth rate constants. We chose those constants from a log-normal distribution parametrized in terms of a mean and coefficient of variation, constraining the coefficient of variation to be no greater than one. These choices were motivated by a recent statistical analysis of patient-specific growth parameters for a very wide variety of cancer types [44]. Again, taking the time for tumor detection to be $\frac{1}{k}ln[\frac{w}{z}]$, but treating *w/z* as a constant, and choosing *k* from the appropriate distribution, we ended up with a survival function of

$$\rho+\frac{1}{2}(1-\rho)Erfc[\frac{\ln(\frac{t}{\phi})-\chi^2}{2\chi}]$$

where *Erfc* is the error function complement, ρ is the fraction of patients not at risk, ϕ is the fold change between starting tumor size and the detection threshold (i.e., *w/z*), and χ varies monotonically with the coefficient of variation of the log normal distribution ($\chi=\sqrt{\frac{1}{2}\ln(1+c^2)}$, where c is the coefficient of variation).

Supplementary Material

Figure S1. Fitting additional cancer recurrence data sets to stochastic and deterministic models. Data were analyzed as in Figure 7D-M.

Table 1. Simulation parameters

Table 2. Cancer data sets used in Fig. 7 and Fig. S1

Table 3. Parameters obtained by data fitting (Fig. 7 and S1).

Acknowledgements

This work was supported by NIH grant U54 CA217378. MGC was supported by training grants T32 EB009418 and T32 GM136624. We thank Genti Buzi for helpful advice.

References

1. Getto P, Marciniak-Czochra A. Mathematical Modelling as a Tool to Understand Cell Self-renewal and Differentiation. Methods Mol Biol. 2015;1293:247-66. doi: 10.1007/978-1-4939-2519-3_15. PubMed PMID: 26040693.
2. Kirouac DC, Madlambayan GJ, Yu M, Sykes EA, Ito C, Zandstra PW. Cell-cell interaction networks regulate blood stem and progenitor cell fate. Mol Syst Biol. 2009;5:293. Epub 2009/07/30. doi: 10.1038/msb.2009.49. PubMed PMID: 19638974; PMCID: 2724979.
3. Rodriguez-Brenes IA, Komarova NL, Wodarz D. Evolutionary dynamics of feedback escape and the development of stem-cell-driven cancers. Proc Natl Acad Sci U S A. 2011;108(47):18983-8. doi: 10.1073/pnas.1107621108. PubMed PMID: 22084071; PMCID: PMC3223454.
4. Lander AD, Gokoffski KK, Wan FY, Nie Q, Calof AL. Cell lineages and the logic of proliferative control. PLoS Biol. 2009;7(1):e15. Epub 2009/01/27. doi: 10.1371/journal.pbio.1000015. PubMed PMID: 19166268.
5. Buzi G, Lander AD, Khammash M. Cell lineage branching as a strategy for proliferative control. BMC Biol. 2015;13:13. doi: 10.1186/s12915-015-0122-8. PubMed PMID: 25857410; PMCID: 4378012.
6. Clayton E, Doupe DP, Klein AM, Winton DJ, Simons BD, Jones PH. A single type of progenitor cell maintains normal epidermis. Nature. 2007;446(7132):185-9. Epub 2007/03/03. doi: 10.1038/nature05574. PubMed PMID: 17330052.
7. Snippert HJ, van der Flier LG, Sato T, van Es JH, van den Born M, Kroon-Veenboer C, Barker N, Klein AM, van Rheenen J, Simons BD, Clevers H. Intestinal crypt homeostasis results from neutral competition between symmetrically dividing Lgr5 stem cells. Cell. 2010;143(1):134-44. Epub 2010/10/05. doi: 10.1016/j.cell.2010.09.016. PubMed PMID: 20887898.
8. Tallapragada NP, Cambra HM, Wald T, Keough Jalbert S, Abraham DM, Klein OD, Klein AM. Inflation-collapse dynamics drive patterning and morphogenesis in intestinal organoids. Cell Stem Cell. 2021;28(9):1516-32 e14. Epub 20210428. doi: 10.1016/j.stem.2021.04.002. PubMed PMID: 33915079; PMCID: PMC8419000.
9. Rompolas P, Mesa KR, Kawaguchi K, Park S, Gonzalez D, Brown S, Boucher J, Klein AM, Greco V. Spatiotemporal coordination of stem cell commitment during epidermal homeostasis. Science. 2016;352(6292):1471-4. Epub 20160526. doi: 10.1126/science.aaf7012. PubMed PMID: 27229141; PMCID: PMC4958018.
10. Gokoffski KK, Kawauchi S, Wu HH, Santos R, Hollenbeck PLW, Lander AD, Calof AL. Feedback Regulation of Neurogenesis in the Mammalian Olfactory Epithelium: New Insights from Genetics and Systems Biology. In: Menini A, editor. The Neurobiology of Olfaction. 2011/09/02 ed. Boca Raton (FL): CRC Press; 2010.
11. Manceau M, Gros J, Savage K, Thome V, McPherron A, Paterson B, Marcelle C. Myostatin promotes the terminal differentiation of embryonic muscle progenitors. Genes Dev. 2008;22(5):668-81. Epub 2008/03/05. doi: 10.1101/gad.454408. PubMed PMID: 18316481.
12. Marciniak-Czochra A, Stiehl T, Ho AD, Jager W, Wagner W. Modeling of asymmetric cell division in hematopoietic stem cells--regulation of self-renewal is essential for efficient repopulation. Stem Cells Dev. 2009;18(3):377-85. Epub 2008/08/30. doi: 10.1089/scd.2008.0143. PubMed PMID: 18752377.
13. Gupta A, Khammash M. Universal structural requirements for maximal robust perfect adaptation in biomolecular networks. Proc Natl Acad Sci U S A. 2022;119(43):e2207802119. Epub 20221018. doi: 10.1073/pnas.2207802119. PubMed PMID: 36256812; PMCID: PMC9618122.

14. Kunche S, Yan H, Calof AL, Lowengrub JS, Lander AD. Feedback, Lineages and Self-Organizing Morphogenesis. PLoS Comput Biol. 2016;12(3):e1004814. doi: 10.1371/journal.pcbi.1004814. PubMed PMID: 26989903; PMCID: PMC4798729.
15. Gokoffski KK, Wu HH, Beites CL, Kim J, Kim EJ, Matzuk MM, Johnson JE, Lander AD, Calof AL. Activin and GDF11 collaborate in feedback control of neuroepithelial stem cell proliferation and fate. Development. 2011;138(19):4131-42. Epub 2011/08/20. doi: 10.1242/dev.065870. PubMed PMID: 21852401; PMCID: 3171217.
16. Lo WC, Chou CS, Gokoffski KK, Wan FY, Lander AD, Calof AL, Nie Q. Feedback regulation in multistage cell lineages. Math Biosci Eng. 2009;6(1):59-82. Epub 2009/03/19. PubMed PMID: 19292508.
17. Lander AD. Pattern, growth, and control. Cell. 2011;144(6):955-69. Epub 2011/03/19. doi: 10.1016/j.cell.2011.03.009. PubMed PMID: 21414486; PMCID: 3128888.
18. Wang MX, Lander A, Lai PY. Regulatory feedback effects on tissue growth dynamics in a two-stage cell lineage model. Phys Rev E. 2021;104(3-1):034405. doi: 10.1103/PhysRevE.104.034405. PubMed PMID: 34654185; PMCID: PMC8585573.
19. Chen CC, Wang L, Plikus MV, Jiang TX, Murray PJ, Ramos R, Guerrero-Juarez CF, Hughes MW, Lee OK, Shi S, Widelitz RB, Lander AD, Chuong CM. Organ-level quorum sensing directs regeneration in hair stem cell populations. Cell. 2015;161(2):277-90. doi: 10.1016/j.cell.2015.02.016. PubMed PMID: 25860610; PMCID: PMC4393531.
20. Fearon ER, Vogelstein B. A genetic model for colorectal tumorigenesis. Cell. 1990;61(5):759-67. doi: 10.1016/0092-8674(90)90186-i. PubMed PMID: 2188735.
21. Tomasetti C, Marchionni L, Nowak MA, Parmigiani G, Vogelstein B. Only three driver gene mutations are required for the development of lung and colorectal cancers. Proc Natl Acad Sci U S A. 2015;112(1):118-23. doi: 10.1073/pnas.1421839112. PubMed PMID: 25535351; PMCID: PMC4291633.
22. Feinberg AP, Levchenko A. Epigenetics as a mediator of plasticity in cancer. Science. 2023;379(6632):eaaw3835. Epub 20230210. doi: 10.1126/science.aaw3835. PubMed PMID: 36758093; PMCID: PMC10249049.
23. Baylin SB, Jones PA. Epigenetic Determinants of Cancer. Cold Spring Harb Perspect Biol. 2016;8(9). Epub 20160901. doi: 10.1101/cshperspect.a019505. PubMed PMID: 27194046; PMCID: PMC5008069.
24. Hitchins MP. Constitutional epimutation as a mechanism for cancer causality and heritability? Nat Rev Cancer. 2015;15(10):625-34. Epub 20150918. doi: 10.1038/nrc4001. PubMed PMID: 26383139.
25. Gueant JL, Chery C, Oussalah A, Nadaf J, Coelho D, Josse T, Flayac J, Robert A, Koscinski I, Gastin I, Filhine-Tresarrieu P, Pupavac M, Brebner A, Watkins D, Pastinen T, Montpetit A, Hariri F, Tregouet D, Raby BA, Chung WK, Morange PE, Froese DS, Baumgartner MR, Benoist JF, Ficicioglu C, Marchand V, Motorin Y, Bonnemains C, Feillet F, Majewski J, Rosenblatt DS. APRDX1 mutant allele causes a MMACHC secondary epimutation in cblC patients. Nat Commun. 2018;9(1):67. Epub 20180104. doi: 10.1038/s41467-017-02306-5. PubMed PMID: 29302025; PMCID: PMC5754367.
26. Tunstrom K, Katz Y, Ioannou CC, Huepe C, Lutz MJ, Couzin ID. Collective states, multistability and transitional behavior in schooling fish. PLoS Comput Biol. 2013;9(2):e1002915. Epub 20130228. doi: 10.1371/journal.pcbi.1002915. PubMed PMID: 23468605; PMCID: PMC3585391.
27. Schweisguth F, Corson F. Self-Organization in Pattern Formation. Dev Cell. 2019;49(5):659-77. doi: 10.1016/j.devcel.2019.05.019. PubMed PMID: 31163171.
28. Brock A, Krause S, Ingber DE. Control of cancer formation by intrinsic genetic noise and microenvironmental cues. Nat Rev Cancer. 2015;15(8):499-509. Epub 20150709. doi: 10.1038/nrc3959. PubMed PMID: 26156637.
29. Liu J, He M, Wang Z, Li Q, Xu B. Current Research Status of Metronomic Chemotherapy in Combination Treatment of Breast Cancer. Oncol Res Treat. 2022;45(11):681-92. Epub 20220819. doi: 10.1159/000526481. PubMed PMID: 35988534; PMCID: PMC9677858.
30. Liu CT, Hsieh MC, Su YL, Hung CM, Pei SN, Liao CK, Tsai YF, Liao HY, Liu WC, Chiu CC, Wu SC, Wang SH, Wei CT, Rau KM. Metronomic vinorelbine is an excellent and safe treatment for advanced breast cancer: a retrospective, observational study. J Cancer. 2021;12(17):5355-64. Epub 20210703. doi: 10.7150/jca.60682. PubMed PMID: 34335952; PMCID: PMC8317530.
31. Gnoni A, Silvestris N, Licchetta A, Santini D, Scartozzi M, Ria R, Pisconti S, Petrelli F, Vacca A, Lorusso V. Metronomic chemotherapy from rationale to clinical studies: a dream or reality? Crit Rev Oncol Hematol. 2015;95(1):46-61. Epub 20150120. doi: 10.1016/j.critrevonc.2015.01.008. PubMed PMID: 25656744.
32. Hanahan D, Bergers G, Bergsland E. Less is more, regularly: metronomic dosing of cytotoxic drugs can target tumor angiogenesis in mice. J Clin Invest. 2000;105(8):1045-7. doi: 10.1172/JCI9872. PubMed PMID: 10772648; PMCID: PMC300842.
33. Mintz B, Illmensee K. Normal genetically mosaic mice produced from malignant teratocarcinoma cells. Proc Natl Acad Sci U S A. 1975;72(9):3585-9. doi: 10.1073/pnas.72.9.3585. PubMed PMID: 1059147; PMCID: PMC433040.
34. Thomas GA, Williams D, Williams ED. Reversibility of the malignant phenotype in monoclonal tumours in the mouse. Br J Cancer. 1991;63(2):213-6. doi: 10.1038/bjc.1991.51. PubMed PMID: 1997097; PMCID: PMC1971777.
35. Maffini MV, Calabro JM, Soto AM, Sonnenschein C. Stromal regulation of neoplastic development: age-dependent normalization of neoplastic mammary cells by mammary stroma. The American journal of pathology. 2005;167(5):1405-10. doi: 10.1016/S0002-9440(10)61227-8. PubMed PMID: 16251424; PMCID: PMC1603788.
36. Brodeur GM. Spontaneous regression of neuroblastoma. Cell Tissue Res. 2018;372(2):277-86. Epub 20180105. doi: 10.1007/s00441-017-2761-2. PubMed PMID: 29305654; PMCID: PMC5920563.
37. Risson E, Nobre AR, Maguer-Satta V, Aguirre-Ghiso JA. The current paradigm and challenges ahead for the dormancy of disseminated tumor cells. Nat Cancer. 2020;1(7):672-80. Epub 20200706. doi: 10.1038/s43018-020-0088-5. PubMed PMID: 33681821; PMCID: PMC7929485.
38. Irvine KD, Shraiman BI. Mechanical control of growth: ideas, facts and challenges. Development. 2017;144(23):4238-48. doi: 10.1242/dev.151902. PubMed PMID: 29183937; PMCID: PMC5769630.
39. Carlson JM, Doyle J. Complexity and robustness. Proc Natl Acad Sci U S A. 2002;99 Suppl 1:2538-45. Epub 2002/03/05. doi: 10.1073/pnas.012582499. PubMed PMID: 11875207.
40. Martincorena I, Roshan A, Gerstung M, Ellis P, Van Loo P, McLaren S, Wedge DC, Fullam A, Alexandrov LB, Tubio JM, Stebbings L, Menzies A, Widaa S, Stratton MR, Jones PH, Campbell PJ. Tumor evolution. High burden and pervasive positive selection of somatic mutations in normal human skin. Science. 2015;348(6237):880-6. doi: 10.1126/science.aaa6806. PubMed PMID: 25999502; PMCID: PMC4471149.
41. Lee-Six H, Olafsson S, Ellis P, Osborne RJ, Sanders MA, Moore L, Georgakopoulos N, Torrente F, Noorani A, Goddard M, Robinson P, Coorens THH, O'Neill L, Alder C, Wang J, Fitzgerald RC, Zilbauer M, Coleman N, Saeb-Parsy K, Martincorena I, Campbell PJ, Stratton MR. The landscape of somatic mutation in normal colorectal epithelial cells. Nature. 2019;574(7779):532-7. Epub 20191023. doi: 10.1038/s41586-019-1672-7. PubMed PMID: 31645730.

42. Soto AM, Sonnenschein C. The somatic mutation theory of cancer: growing problems with the paradigm? Bioessays. 2004;26(10):1097-107. doi: 10.1002/bies.20087. PubMed PMID: 15382143.
43. Rueda OM, Sammut SJ, Seoane JA, Chin SF, Caswell-Jin JL, Callari M, Batra R, Pereira B, Bruna A, Ali HR, Provenzano E, Liu B, Parisien M, Gillett C, McKinney S, Green AR, Murphy L, Purushotham A, Ellis IO, Pharoah PD, Rueda C, Aparicio S, Caldas C, Curtis C. Dynamics of breast-cancer relapse reveal late-recurring ER-positive genomic subgroups. Nature. 2019;567(7748):399-404. Epub 20190313. doi: 10.1038/s41586-019-1007-8. PubMed PMID: 30867590; PMCID: PMC6647838.
44. Kay K, Dolcy K, Bies R, Shah DK. Estimation of Solid Tumor Doubling Times from Progression-Free Survival Plots Using a Novel Statistical Approach. AAPS J. 2019;21(2):27. Epub 20190208. doi: 10.1208/s12248-019-0302-5. PubMed PMID: 30737615; PMCID: PMC8383152.

Table 1. Parameters used in simulations

	p0	γ	*k*	ϕ	*n1*	*n2*	*d*	*c0* initial conditions	*c1* initial conditions	λ (cell radius)
Fig. 1A								500	1000	
Fig. 1B								500	1000	
Fig. 2B	0.85	0.0025		0.0	1	1	0.25	1	0	
Fig. 2C	0.85	0.0025		0.0	1	1	0.25	$10^{0.1}$ and 10	$10^{0.1}$ and 10^{3}	
Fig. 2D	0.85	0.0025		0.0	1	1	0.25	1	0	
Fig. 2F	0.85	0.001		0.0	1	1	0.0	1	0	
Fig. 2G	0.85	0.001		0.0	1	1	0.0	$10^{0.1}$ and $10^{2.5}$	$10^{0.1}$ and $10^{0.1}$	
Fig. 2H	0.85	0.001		0.0	1	1	0.0	1	0	
Fig. 2J	0.9		0.7	0.0	1	1	0.0	1	0	100 (5)
Fig. 2J'	0.9		0.9	0.0	1	1	0.0	1	0	100 (5)
Fig. 2K	0.9		0.4	0.0	1	1	0.5	10 and 30000	0.1 and 1000	100 (5)
Fig. 2N	0.9		0.75	0.0	1	1	0.0	1	0	100 (5)
Fig. 2N'	0.9		1.3	0.0	1	1	0.0	1	0	100 (5)
Fig. 2O	0.9		0.3	0.0	1	1	0.0	1 and 10	0.1 and 20	100 (5)
Fig. 3	1.0		0.14	0.0	1	1	0.0			λ = 2 cell diameters
Fig. 4B	0.9		0.4	0.0	1	1	0.2	$10^{0.1}$ and $10^{2.0}$	$10^{0.01}$ and $10^{0.01}$	22.5 (5)
Fig. 4C	0.9		0.4	0.0	1	1	0.2	1	0	22.5 (5)
Fig. 4E	0.9		0.4	0.0	1	1	0.0	$10^{0.1}$ and $10^{2.2}$	$10^{0.01}$ and $10^{0.01}$	22.5 (5)
Fig. 4F	0.9		0.4	0.0	1	1	0.0	1	0	22.5 (5)
Fig. 4H	0.9		0.4	0.0	1	1	0.35	10^{1} and 10^{3}	$10^{0.1}$ and $10^{0.1}$	35 (5)
Fig. 4I	0.9		0.4	0.0	1	1	0.35	1	0	35 (5)

Fig. 4K	0.9		0.4	0.0	1	1	0.0	$10^{0.1}$ and $10^{2.0}$	$10^{0.1}$ and $10^{0.1}$	22.5 (5)
Fig. 4L	0.9		0.4	0.0	1	1	0.0	1	0	22.5 (5)
Fig. 5B	0.85	0.006		0.0003	1	1.75	0.0	$10^{0.1}$ and $10^{2.8}$	$10^{0.1}$ and $10^{2.8}$	
Fig. 5C	0.85	0.006		0.0003	1	1.75	0.0	1	0	
Fig. 5E	0.8	0.006		0.00085	1	1.5	0.4	$10^{0.1}$ and $10^{2.8}$	$10^{0.1}$ and $10^{2.8}$	
Fig. 5F	0.8	0.006		0.00085	1	1.5	0.4	1	0	
Fig. 5H	0.8	0.004		0.001	1	1.25	0.15	$10^{0.1}$ and $10^{3.0}$	$10^{0.1}$ and $10^{0.1}$	
Fig. 5I	0.8	0.004		0.001	1	1.25	0.15	1	0	
Fig. 6A	0.9	0.0008		$6.15926*10^{-5}$	1	1.3	0.2	700	3300	
Fig. 6B	0.9	0.0008		$6.15926*10^{-5}$	1	1.3	0.2	1215	6075	
Fig. 6C	0.9	0.0008		$6.15926*10^{-5}$	1	1.3	0.2	240	1200	
Fig. 6D	0.9	0.0008		$6.15926*10^{-5}$	1	1.3	0.2	45	225	
Fig. 6E	0.9	0.0008		$6.15926*10^{-5}$	1	1.3	0.2	7500	7500	
Fig. 6F	0.9	0.0008		$6.15926*10^{-5}$	1	1.3	0.2	7500	7500	
Fig. 6G	0.9	0.0008		$6.15926*10^{-5}$	1	1.3	0.2	7500	7500	
Fig. 6H	0.9	0.0008		$6.15926*10^{-5}$	1	1.3	0.2			
Fig. 6I	0.9	0.0008		$6.15926*10^{-5}$	1	1.3	0.2			
Fig. 6J	0.9	0.0008		$6.15926*10^{-5}$	1	1.3	0.2			

TABLE 2: Sources of cancer recurrence data for Figures 7 and Supplemental Figure 1.

Cancer Type	Prior treatment	Criterion	Study Population Size	Citation
Chronic myeloid leukemia (CML) (STIM2 trial)	Imatinib (study begins after discontinuation)	molecular recurrence-free survival	199	(Dulucq et al., 2022)
Chronic myeloid leukemia (CML) (ENESTfreedom trial)	Nilotinib (study begins after discontinuation)	treatment-free remission	190	(Ureshino, 2021)
Chronic myeloid leukemia (CML) (EURO-SKI trial)	TKI therapy (study begins after discontinuation)	molecular recurrence-free remission	755	(Saussele et al., 2018)
Acute lymphoblastic leukemia (ALL2000)	(Study begins at date of remission – generally induction) Staged Chemotherapy: Induction, consolidation, intensification, irradiation, and maintenance ~6% received SCT	relapse-free survival	1064	(Jensen et al., 2022)
Acute lymphoblastic leukemia (ALL2008)	(Study begins at date of remission – generally induction) Induction and consolidation chemotherapy followed by personalized chemotherapy based on risk status (standard, intermediate and high risk)	relapse-free survival	1752	(Jensen et al., 2022)
Breast Cancer--triple negative 1	(DFS begins at the date of diagnosis) ~95% surgical removal ~97% Chemotherapy: ACT or NACT	disease-free survival	1297	(Bajpai et al., 2022)

	~80% Adjuvent radiotherapy			
Breast Cancer--triple negative 2	(DFS begins at the date of diagnosis) ~99% Surgical removal ~67% Radiotherapy ~75% Chemotherapy	disease-free survival	1374	(Ignatov et al., 2018)
Breast Cancer--triple negative 3	(DFS start time not specified-presumably post-surgery and during chemo) 100% Surgery ~78% adjuvant chemotherapy ~11% neoadjuvant chemotherapy	Incidence of recurrence	702	(Eom et al., 2019)
Breast Cancer--HER2 enriched	(DFS begins at the date of diagnosis) ~98% Surgical removal ~67% Radiotherapy ~76% Chemotherapy	disease-free survival	614	(Ignatov et al., 2018)
Breast Cancer--luminal B-type	(DFS begins at the date of diagnosis) ~97% Surgical removal ~67% Radiotherapy ~45% Chemotherapy ~67% Hormone Therapy	disease-free survival	4122	(Ignatov et al., 2018)
Breast Cancer- ER negative	Not described	Relapse-free survival	186	(Rueda et al., 2019)
Breast Cancer- ER positive	Not described	Relapse-free survival	419	(Rueda et al., 2019)
Prostate cancer	(DFS begins at the date of diagnosis)	cancer-specific-mortality (CS<M)-free survival (2009-2014)	11296	(Bandini et al., 2018)

	21% prostatectomy radiotherapy or combined ~ 72% no-local treatment Anti-androgen Therapy Docetaxel, cabazitaxel, sipuleuecel-T, abiraterone, and enzalutamide			
Colorectal cancer, stage 3	(DFS post operative) 100% Surgical removal ~74% Adjuvant Chemotherapy	loco-regional recurrence free survival	416	(Liska et al., 2017)
Renal cell carcinoma	(DFS begins at surgery date) Surgery ~90% of which was Radical Nephrectomy	disease free survival	3024	(Marconi et al., 2021)
Renal cell carcinoma	(OS begins from time of treatment) Nephrectomy	Overall survival	477	(Zisman et al., 2001)
Renal cell carcinoma	(DFS begin post surgery) Nephrectomy	Disease-free survival	299	(Brookman-Amissah et al., 2009)
Primary Basal Cell Carcinoma	(DFS begins post treatment) Curettage Electrodesiccation, Surgical Excision, or X-Ray Therapy	disease-free survival	3764	(Silverman et al., 1991)

Hepatocellular Carcinoma	(Study begins post liver transplant) Liver transplant	recurrence free survival	4980	(Tran et al., 2023)
Hepatocellular Carcinoma	(Study begins post surgery) Hepatic resection	Disease free survival	241	(Sakon et al., 2000)
Melanoma	(Study begins post excision) Surgical Excision	local recurrence-free survival	1041	(Zalaudek et al., 2003)
Ovary	(Study begins at 15'th of the month of diagnosis) Received chemo and surgery; displayed recurrence and then received chemo	relapse-free survival	2038	(Bickell et al., 2018)
Ovary	(DFS begins at the time of remission) Chemotherapy	Disease-free survival	140 (65+) 96 (45-55)	(Kurta et al., 2014)

References

Bajpai, J., L. Kashyap, D.H. Vallathol, A. Das, M. Singh, R. Pathak, S. Rath, A. Sekar, S. Mohanta, A. Reddy, S. Joshi, R. Nandhana, R. Ravind, T. Wadasadawala, N. Nair, J. Ghosh, V. Parmar, S. Gulia, S. Desai, T. Shet, M. Thakur, A. Patil, R. Sarin, S. Gupta, and R. Badwe. 2022. Outcomes of non-metastatic triple negative breast cancers: Real-world data from a large Indian cohort. *Breast*. 63:77-84.

Bandini, M., R.S. Pompe, M. Marchioni, E. Zaffuto, G. Gandaglia, N. Fossati, L. Cindolo, F. Montorsi, A. Briganti, F. Saad, and P.I. Karakiewicz. 2018. Improved cancer-specific free survival and overall free survival in contemporary metastatic prostate cancer patients: a population-based study. *Int Urol Nephrol*. 50:71-78.

Bickell, N.A., N. Egorova, M. Prasad-Hayes, R. Franco, E.A. Howell, J. Wisnivesky, and P. Deb. 2018. Secondary Surgery Versus Chemotherapy for Recurrent Ovarian Cancer. *Am J Clin Oncol*. 41:458-464.

Brookman-Amissah, S., F. Kendel, I. Spivak, S. Pflanz, J. Roigas, T. Klotz, and M. May. 2009. Impact of clinical variables on predicting disease-free survival of patients with surgically resected renal cell carcinoma. *BJU Int*. 103:1375-1380.

Dulucq, S., F.E. Nicolini, D. Rea, P. Cony-Makhoul, A. Charbonnier, M. Escoffre-Barbe, V. Coiteux, P. Lenain, F. Rigal-Huguet, J. Liu, A. Guerci-Bresler, L. Legros, J.C. Ianotto, M. Gardembas, P. Turlure, V. Dubruille, P. Rousselot, J. Martiniuc, H. Jardel, H. Johnson-Ansah, B. Joly, T. Henni, E. Cayssials, P. Zunic, M.G. Berger, B. Villemagne, F. Robbesyn, S. Morisset, F.X. Mahon, and G. Etienne. 2022. Kinetics of early and late molecular recurrences after first-line imatinib cessation in chronic myeloid leukemia: updated results from the STIM2 trial. *Haematologica*. 107:2859-2869.

Eom, H., C. JH, C. WJ, C. EY, S. HJ, and H. Kim. 2019. Recurrence in Stage I and II Triple-Negative Breast Cancer: Analysis of Clinicopathologic and Imaging Factors. *Research Square*.

Ignatov, A., H. Eggemann, E. Burger, and T. Ignatov. 2018. Patterns of breast cancer relapse in accordance to biological subtype. *J Cancer Res Clin Oncol*. 144:1347-1355.

Jensen, K.S., T. Oskarsson, P.M. Lahteenmaki, T. Flaegstad, O.G. Jonsson, P. Svenberg, K. Schmiegelow, M. Heyman, U. Noren-Nystrom, H. Schroder, and B.K. Albertsen. 2022. Temporal changes in incidence of relapse and outcome after relapse of childhood acute lymphoblastic leukemia over three decades; a Nordic population-based cohort study. *Leukemia*. 36:1274-1282.

Kurta, M.L., R.P. Edwards, K.B. Moysich, K. McDonough, M. Bertolet, J.L. Weissfeld, J.M. Catov, F. Modugno, C.H. Bunker, R.B. Ness, and B. Diergaarde. 2014. Prognosis and conditional disease-free survival among patients with ovarian cancer. *J Clin Oncol*. 32:4102-4112.

Liska, D., L. Stocchi, G. Karagkounis, F. Elagili, D.W. Dietz, M.F. Kalady, H. Kessler, F.H. Remzi, and J. Church. 2017. Incidence, Patterns, and Predictors of Locoregional Recurrence in Colon Cancer. *Ann Surg Oncol*. 24:1093-1099.

Marconi, L., M. Sun, C. Beisland, T. Klatte, B. Ljungberg, G.D. Stewart, S. Dabestani, T.K. Choueiri, and A. Bex. 2021. Prevalence, Disease-free, and Overall Survival of Contemporary Patients With Renal Cell Carcinoma Eligible for Adjuvant Checkpoint Inhibitor Trials. *Clin Genitourin Cancer*. 19:e92-e99.

Rueda, O.M., S.J. Sammut, J.A. Seoane, S.F. Chin, J.L. Caswell-Jin, M. Callari, R. Batra, B. Pereira, A. Bruna, H.R. Ali, E. Provenzano, B. Liu, M. Parisien, C. Gillett, S. McKinney, A.R. Green, L. Murphy, A. Purushotham, I.O. Ellis, P.D. Pharoah, C. Rueda, S. Aparicio, C. Caldas, and C. Curtis. 2019. Dynamics of breast-cancer relapse reveal late-recurring ER-positive genomic subgroups. *Nature*. 567:399-404.

Sakon, M., K. Umeshita, H. Nagano, H. Eguchi, S. Kishimoto, A. Miyamoto, S. Ohshima, K. Dono, S. Nakamori, M. Gotoh, and M. Monden. 2000. Clinical significance of hepatic resection in hepatocellular carcinoma: analysis by disease-free survival curves. *Arch Surg*. 135:1456-1459.

Saussele, S., J. Richter, J. Guilhot, F.X. Gruber, H. Hjorth-Hansen, A. Almeida, J. Janssen, J. Mayer, P. Koskenvesa, P. Panayiotidis, U. Olsson-Stromberg, J. Martinez-Lopez, P. Rousselot, H. Vestergaard, H. Ehrencrona, V. Kairisto, K. Machova Polakova, M.C. Muller, S. Mustjoki, M.G. Berger, A. Fabarius, W.K. Hofmann, A. Hochhaus, M. Pfirrmann, F.X. Mahon, and E.-S. investigators. 2018. Discontinuation of tyrosine kinase inhibitor therapy in chronic myeloid leukaemia (EURO-SKI): a prespecified interim analysis of a prospective, multicentre, non-randomised, trial. *The Lancet. Oncology*. 19:747-757.

Silverman, M.K., A.W. Kopf, C.M. Grin, R.S. Bart, and M.J. Levenstein. 1991. Recurrence rates of treated basal cell carcinomas. Part 1: Overview. *J Dermatol Surg Oncol*. 17:713-718.

Tran, B.V., D. Moris, D. Markovic, H. Zaribafzadeh, R. Henao, Q. Lai, S.S. Florman, P. Tabrizian, B. Haydel, R.M. Ruiz, G.B. Klintmalm, D.D. Lee, C.B. Taner, M. Hoteit, M.H. Levine, U. Cillo, A. Vitale, E.C. Verna, K.J. Halazun, A.D. Tevar, A. Humar, W.C. Chapman, N. Vachharajani, F. Aucejo, J. Lerut, O. Ciccarelli, M.H. Nguyen, M.L. Melcher, A. Viveiros, B. Schaefer, M. Hoppe-Lotichius, J. Mittler, T.L. Nydam, J.F. Markmann, M. Rossi, C. Mobley, M. Ghobrial, A.N. Langnas, C.A. Carney, J. Berumen, G.T. Schnickel, D.L. Sudan, J.C. Hong, A. Rana, C.M. Jones, T.M. Fishbein, R.W. Busuttil, A.S. Barbas, and V.G. Agopian. 2023. Development and validation of a REcurrent Liver cAncer

Prediction ScorE (RELAPSE) following liver transplantation in patients with hepatocellular carcinoma: Analysis of the US Multicenter HCC Transplant Consortium. *Liver Transpl*. 29:683-697.
Ureshino, H. 2021. Treatment-free remission and immunity in chronic myeloid leukemia. *Int J Hematol*. 113:642-647.
Zalaudek, I., M. Horn, E. Richtig, S. Hodl, H. Kerl, and J. Smolle. 2003. Local recurrence in melanoma in situ: influence of sex, age, site of involvement and therapeutic modalities. *Br J Dermatol*. 148:703-708.
Zisman, A., A.J. Pantuck, F. Dorey, J.W. Said, O. Shvarts, D. Quintana, B.J. Gitlitz, J.B. deKernion, R.A. Figlin, and A.S. Belldegrun. 2001. Improved prognostication of renal cell carcinoma using an integrated staging system. *J Clin Oncol*. 19:1649-1657.

Table 2. Best fit parameters from fitting models 1, 2 and 3 to recurrance data

		model 1			model 2			model 3		
		k	α	ρ	k	μ	ρ	ϕ	χ	ρ
Chronic myeloid leukemia CML STIM2 trial	Dulucq et al., 2022	0.19	0.796	0.467	0.507	0.131	0.487	4.042	0.355	0.484
Chronic myeloid leukemia CML ENESTfreedom trial	Ureshino, 2021	0.057	0.883	0.457	0.174	0.105	0.552	13.341	0.314	0.549
Chronic myeloid leukemia CML EURO-SKI trial	Saussele et al., 2018	0.347	0.942	0.519	0.538	0.3	0.533	1.88	0.549	0.522
Acute lymphoblastic leukemia ALL2000	Jensen et al., 2022	0.462	0.998	0.728	0.952	0.333	0.764	1	0.589	0.744
Acute lymphoblastic leukemia ALL2008	Jensen et al., 2022	0.244	0.99	0.78	0.63	0.333	0.844	1.373	0.589	0.84
Breast Cancer--triple negative	Bajpai et al., 2022	0.027	0.958	0.536	0.052	0.333	0.593	17.156	0.589	0.574
Breast Cancer--triple negative	Ignatov et al., 2018	0.504	0.963	0.786	0.86	0.271	0.8	1.346	0.514	0.793
Breast Cancer--triple negative	Eom et al., 2021	0.033	0.957	0.804	0.049	0.333	0.817	18.175	0.589	0.807
Breast Cancer--HER2 enriched	Eom et al., 2021	0.136	0.981	0.713	0.309	0.318	0.783	3.136	0.589	0.765
Breast Cancer--luminal B-type	Ignatov et al., 2018	0.194	0.965	0.851	0.416	0.285	0.878	2.689	0.563	0.866
Breast Cancer--ER negative	Eom et al., 2021	0.404	0.904	0	1.009	0.246	0.5	1.996	0.505	0.885
Breast Cancer--ER positive	Eom et al., 2021	0.404	0.904	0	1.009	0.246	0.5	1.997	0.506	0.886
Prostate cancer	Bandini et al., 2018	0.025	0.986	0.163	0.062	0.333	0.364	14.363	0.589	0.334
Colorectal cancer, stage 3	Liska et al., 2017	0.394	0.972	0.887	0.796	0.333	0.904	1.126	0.589	0.899
Renal cell carcinoma	Marconi et al., 2021	0.02	0.949	0.559	0.048	0.333	0.616	17.49	0.589	0.608
Renal cell carcinoma	Zisman et al., 2001	0.035	0.968	0.327	0.076	0.333	0.396	10.961	0.589	0.385
Renal cell carcinoma	Brookman-Amissah et al., 2009	0.021	0.887	0.487	0.053	0.333	0.56	14.842	0.589	0.558
Primary Basal Cell Carcinoma	Silverman et al., 1991	0.239	0.992	0.847	0.545	0.333	0.871	1.592	0.589	0.866
Hepatocellular Carcinoma	Tran et al., 2023	0.041	0.978	0.867	0.078	0.333	0.884	11.268	0.589	0.879
Hepatocellular Carcinoma	Sakon et al., 2000	0.346	0.985	0.157	0.688	0.333	0.241	1.243	0.589	0.221
Melanoma	Zalaudek et al., 2003	0.021	0.949	0.931	0.044	0.333	0.942	20.425	0.589	0.939
Ovarian age 65+	Kurta et al., 2014	0.889	0.97	0.34	1.4	0.333	0.333	1	0.589	0.163
Ovarian age 45-55	Kurta et al., 2014	0.489	0.948	0.48	1.206	0.333	0.567	1	0.589	0.48
Ovarian, second relapse	Bickell et al., 2018	0.288	0.94	0	0.506	0.265	0.061	2.393	0.518	0